Korean J. Chem. Eng., 40(5), 1103-1115 (2023)
DOI: 10.1007/s11814-022-1277-y

pISSN: 0256-1115
eISSN: 1975-7220

Ammonia recovery from natural rubber processing wastewater by hollow fiber membrane contactors: Mass transfer in short- and long-term operations and fouling characteristics

Nattakan Janchuaina*,, Nititorn Chusri***, Ratana Jiraratananon****, Tae-Hyun Bae*****, and Wichitpan Rongwong*,**,†**

*Department of Chemical Engineering and Pharmaceutical Chemistry, School of Engineering and Technology, Walailak University, Tasala, Nakhon Si Thammarat 80161, Thailand
**Biomass and Oil Palm Center of Excellence, Walailak University, Tasala, Nakhon Si Thammarat 80161, Thailand
***The Center for Scientific and Technological Equipment, Walailak University 222 Thai Buri, Tha Sala District, Nakhon Si Thammarat Province 80160 Thailand.0161, Thailand
****Faculty of Engineering, King Mongkut's University of Technology Thonburi, Toongkru, Bangkok 10140, Thailand
*****Department of Chemical and Biomolecular Engineering, Korea Advanced Institute of Science and Technology, Daejeon 34141, Korea

(*Received 3 June 2022 • Revised 24 August 2022 • Accepted 28 August 2022*)

Abstract–This study investigates the performance of hydrophobic membrane contactors (HMC) for the recovery of dissolved ammonia (NH_3) from natural rubber processing (NRP) wastewater during short- and long-term operation. The results show that 90% recovery of total NH_3 nitrogen can be achieved. In the short-term operations, the increases in the wastewater velocity and pH enhanced the NH_3 desorption overall mass transfer coefficient (K_{OV}), but the increase in the number of total solids in the wastewater reduced the K_{OV}. The Wilson plot method confirmed the significance of the mass transfer resistance of the wastewater phase for NH_3 desorption. The long-term operation revealed that the K_{OV} was kept constant for 15 days and then declined owing to membrane fouling. Flushing using water (physical cleaning) could not restore the K_{OV} to its initial value, but a series of chemical cleanings with 0.1 M NaOH and 0.1 M HCl solution successfully recovered the K_{OV}. The comparison of cleaning solutions in the foulant extraction's ability showed that 0.1 M NaOH was the most potent, followed by 0.1 M HCl and water. Fouling characterization using scanning electron microscopy and energy dispersive X-ray spectrometry (SEM/EDS) and the Fourier transform infrared spectroscopy revealed a cake layer covering the membrane surface, and the foulants consisted of organic compounds composed of proteins from natural rubber (NR) particles and inorganic salts. The hydrophobic interaction of the proteins covering the NR particles allowed the natural rubber particles to be deposited on the membrane surface, even without hydraulic pressure in HMC. The negative charge of the NR particles could also interact with ions, leading to the formation of inorganic components in the fouling cake layers. Two types of fouled membrane surfaces were identified via SEM/EDS: a smooth area, which consisted of N-atom from proteins, and a rugged area with small conglomerate particles in which no N-atoms were observed.

Keywords: Ammonia Recovery, Fouling Characteristics, Membrane Contactors, Natural Rubber Wastewater

INTRODUCTION

The natural rubber (NR) industry is a key economic sector for southeast Asian countries, which produced around 75% of global production and generated over 1.35 billion USD in income for the region in 2019 [1]. Natural rubber latex harvested from rubber trees (*Hevea brasiliensis*) is used to produce concentrated latex, block rubber, and ribbed smoked sheets, which are the primary raw materials for many essential commodities, such as automobile tires, gloves, elastics, and condoms.

However, natural latex can coagulate easily, making it difficult to process further. Therefore, ammonia (NH_3), an inexpensive and effective anticoagulant, must be added in significant amounts for latex preservation. For example, 17 kg of NH_3 is required to produce 1 ton of concentrated latex [2]. This results in wastewater associated with natural latex processing containing a considerable amount of dissolved NH_3 and ammonium ions (NH_4^+). Without proper treatment, natural rubber processing (NRP) wastewater can lead to several serious environmental problems, such as deteriorated quality of receiving water, eutrophication, and, in particular, odor problems [3].

Aerobic wastewater treatment systems are commonly employed for NRP wastewater, in which the nitrogen (N) content is treated via the biological nitrification-denitrification process. Although effective, it requires a long operation time and large reactor volume [4]. Although there has been progress in developing treatment tech-

†To whom correspondence should be addressed.
E-mail: wichitpan.ro@wu.ac.th

Table 1. Performance of the hollow fiber membrane contactors (HMC) in treating different types of wastewaters for NH_3 nitrogen removal and the ranges of nitrogen species concentration reported as NH_3 or total NH_3 nitrogen (TAN, NH_4^++NH_3)

Types of wastewater	Nitrogen species concentration	Reported performance	Refs.
Dairy manure/swine manure	102-196 mg/L of NH_3	11-49% NH_3 removal efficiency	[15]
	1,070-2,290 mg/L of TAN	88-94% NH_3 removal efficiency	[16]
	1,430-6,130 mg/L of TAN	3.7-51 g/m^2/day of NH_3 flux	[17]
Human urine (synthetic)	~5,000 mg/L of TAN	33-80.3% NH_3 removal efficiency	[18]
Anaerobic effluent	2,300 mg/L of TAN	70-97% NH_3 removal efficiency	[19]
	3,435 mg/L of TAN	80-98.5% NH_3 removal efficiency	[20]
Poultry litter	1,880-5,110 mg/kg of TAN	70-97% NH_3 removal efficiencyfrom the headspace	[21]
Coking wastewater	648 mg/L of TAN	54% NH_3 removal efficiencyfrom the headspace	[22]
Slaughterhouse wastewater	>2 mg/L of NH_3	64-99.8% NH_3 removal efficiency	[23]
Landfill leachate	881 mg/L as TAN	79.1-96.6 TAN removal efficiency	[24]

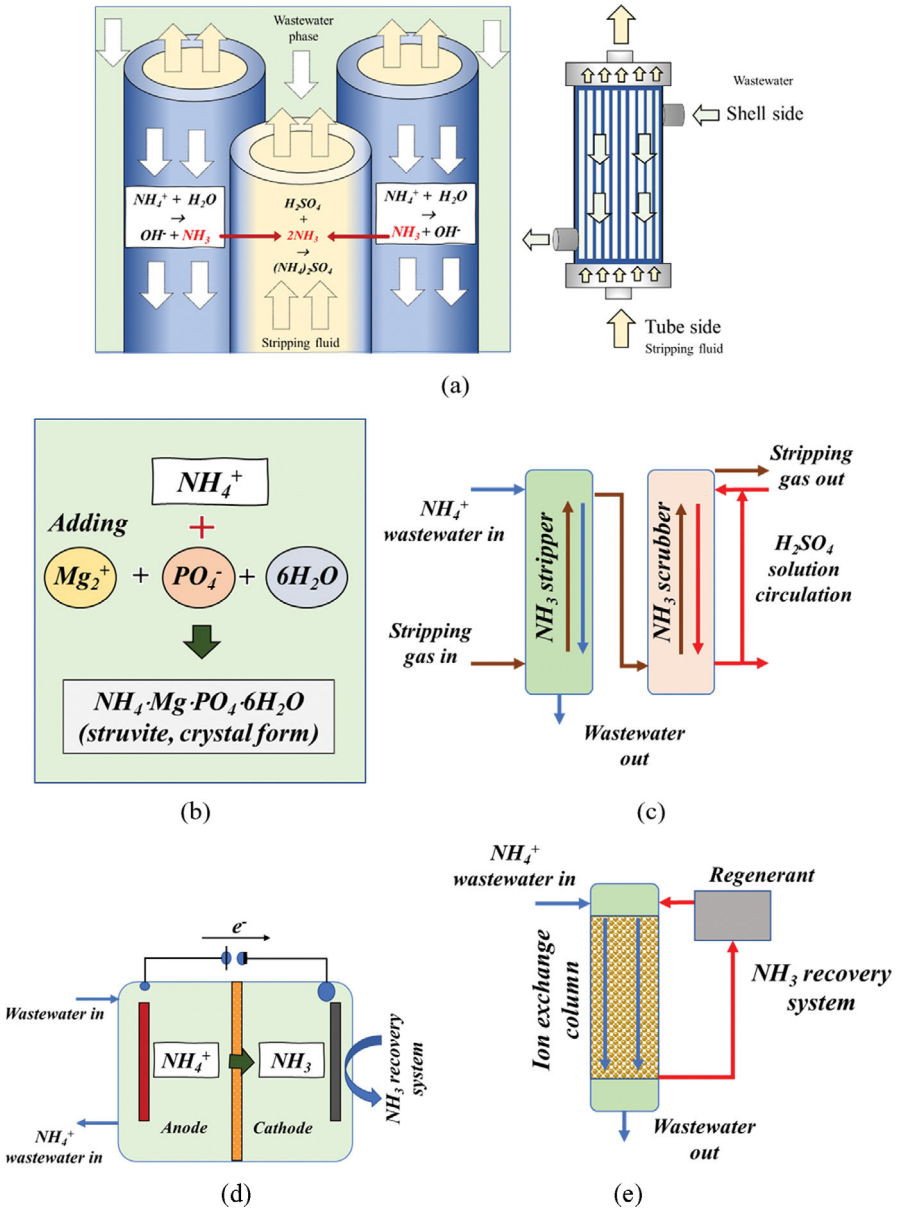

Fig. 1. Physicochemical techniques for ammonia recovery. (a) HMC (b) struvite precipitation (c) gas stripping, (d) bioelectrochemical system and (e) ion exchange.

niques, such as electrochemical techniques [5,6], most NRP wastewater is still treated via an aerobic wastewater system [7]. In addition, N can be converted to nitrous oxide, a potent greenhouse gas that contributes to climate change [8]. Biological processes also only remove NH_3, but cannot transform it into a usable form. As it is present in considerable amounts in NRP wastewater, NH_3 recovery for reuse is preferable to lower the overall treatment cost.

Several physicochemical technologies, such as struvite precipitation, gas stripping, bioelectrochemical systems, and ion exchange have been employed for NH_3 recovery. Among these physicochemical technologies, hydrophobic membrane contactors (HMC) are one of the most promising [9] and have displayed exceptional performance in NH_3 recovery from several types of wastewater (Table 1). HMC employs hydrophobic membranes as phase barriers for the mass transfer of NH_3 between the wastewater and stripping fluid phases. As phase barriers, HMC enables the two phases to contact each other for mass transfer without the dispersion of one phase into the other. Separation selectivity is provided by the affinity of the substance toward the stripping phase, not the membrane itself. This indirect contact between phases provides several advantages: 1) Ease of operation as the flows can be independently adjusted, 2) No phase mixing problems, such as foaming and flooding, which are usually found in the conventional treatment of wastewater with high organic compounds, 3) Straightforward scaling up from the constant and known interfacial area, which can be determined directly from the membrane surface area [10] and 4) Recovered NH_3 separate from wastewater, which makes further processing less complicated. The membrane in the hollow fiber configuration also has the significant advantage of a high interfacial surface-to-volume ratio compared to conventional mass transfer equipment, such as packed or bubble columns. It was reported that HMC unit volumes are 1.4 to 15-times lower than those of packed columns [11].

A schematic diagram of NH_3 recovery using HMC and other physicochemical techniques is displayed in Fig. 1. The dissolved NH_3 in the NRP wastewater is mainly present in NH_4^+ ions because of acidic conditions owing to the addition of sulfuric acid (H_2SO_4) as a coagulant. Therefore, an alkali solution is required to convert NH_4^+ ions to NH_3 in the gaseous dissolved form, as implied by the following equation:

$$NH_{4,(aq)}^{+} + OH^{-} \underset{K_b}{\overset{K_a}{\rightleftharpoons}} NH_{3,(aq)} + H_2O \quad (1)$$

where K_a and K_b are the acid and base dissociation constants, respectively.

Gaseous NH_3 can diffuse through the membrane to the stripping solution because of the concentration difference. It then reacts with H_2SO_4 in the stripping solution to form ammonium sulfate ($(NH_4)_2SO_4$), which can be used as a fertilizer.

HMC was tested for NH_3 recovery from different wastewaters (Table 1). Although NRP wastewater possesses a high amount of dissolved NH_3, making the recovery process easily profitable, it was not previously tested for NH_3 recovery using HMC. Moreover, most NH_3 recovery performances using HMC reported in the literature were from short-term operations. Although HMC has a low membrane fouling tendency from operating under atmospheric pressure conditions, a decline in the performance during long-term operations owing to membrane fouling is inevitable. Therefore, it is essential to investigate the long-term performance, fouling mechanism, and development of membrane cleaning strategies for HMC. This is particularly important because the NRP wastewater contains a considerable quantity of organic compounds in the form of uncoagulated rubber particles.

To the best of our knowledge, this study is the first to propose a recovery process for dissolved NH_3 from NRP wastewater. To date, most NRP wastewater nitrogen treatment research has focused on the use of biological technologies. The examples include the downflow hanging sponge (DHS) reactor [12], which reported an NH_3 nitrogen removal efficiency of 20.8%, and the anaerobic treatment [13], which reported a total Kjeldahl nitrogen (TKN) removal of 80%. Alternatively, the treatment was performed using physicochemical methods, such as adsorption on zeolite [14], which reported an NH_3 nitrogen removal efficiency of 87.2%, and the adsorption on kaolin, which reported an NH_3 nitrogen removal efficiency of 75.8%. For NRP wastewater in which the dissolved NH_3 concentration could be up to 3,000 mg/L, [3] the recovery process could be an opportunity for another income and reduce the cost of the overall treatment process for NR factories. Currently, the most common treatment technologies applied to NRP wastewater are pond treatment systems [13], which focus only on organic pollutant removal. These systems require latex trap pretreatment to remove solid residuals. HMC could be implemented after the latex trap to recover dissolved NH_3 into the usable form of $(NH_4)_2SO_4$ and before the wastewater is treated for organic removal in the following step.

The main aim of this study is to comprehensively examine the performance of HMC for NH_3 recovery from actual NRP wastewater in both short- and long-term operations. The significance of operating parameters on the overall mass transfer coefficients (K_{OV}), including the flow rates, pH, and total solid content of the NRP wastewater, was investigated. The long-term performance of HMC was observed for over 20 days by continuously feeding the HMC' system with the NRP wastewater to investigate the membrane fouling that occurred during the process. Membrane-cleaning strategies have also been proposed to maintain the long-term stability of the system. In addition, the membrane foulants were characterized, and a potential fouling mechanism is proposed. The efficiency of different cleaning solutions in alleviating fouling was also explored. Notably, this is the first study to investigate the fouling mechanism of NRP wastewater on a hydrophobic membrane surface, which will help confirm the feasibility and viability of the HMC process for resource recovery applications.

MATERIALS AND METHODS

1. Natural Rubber Processing Wastewater

NRP wastewater was obtained from TT Latex and Products Co., Ltd. Factory (Nakorn Sri Thammarat). The samples were stored in a refrigerator at 4 °C after receival. The wastewater characteristics are listed in Table 2. Total NH_3 nitrogen (TAN) and total Kjeldahl nitrogen (TKN) were measured using the Nessler and distillation methods. Chemical oxygen (COD), total solids (TS), and total dissolved solids (TDS) were measured using the standard methods of the American Water Works Association (AWWA, 23rd edition [25]).

Table 2. NRP wastewater characteristics

Parameters	Values
pH	2.5±0.5
TAN (mg/L)	600±125
TKN (mg/L)	795±240.5
COD (mg/L)	3,395 ±1,380
TS (mg/L)	6,247±2,127.5
TDS (mg/L)	324.17±34.16
SO_4^{2-} (mg/L)	1,890±62
K (mg/L)	648±6.5
Zn (mg/L)	60.25±24.35
Ca (mg/L)	31.85±0.2
Fe (mg/L)	7.525±4.1
Cu (mg/L)	0.063±0.013

Table 3. Membrane and membrane module properties

Parameters	Values
Number of fibers	25
Total membrane length (m)	0.42
Outside membrane diameter (m)	2.30×10^{-03}
Inside membrane diameter (m)	1.20×10^{-03}
Inside module diameter (m)	1.90×10^{-02}
Membrane porosity (m)	0.45
Membrane pore diameter (m)	2.50×10^{-07}
Log mean diameter (m)	1.69×10^{-03}
Packing density	0.372
Total membrane surface (outer side, m^2)	0.076

All positive discharge ions in the NRP wastewater were analyzed by inductively coupled plasma-mass spectrometry (Perkin Elmer, Avio200).

2. The Membrane Contactor and Set Up

2-1. The Membrane

The membrane used was a commercial polytetrafluoroethylene (PTFE) hydrophobic microporous hollow fiber obtained from Altrateck (China). Membrane modules were constructed by plotting the fibers with an epoxy-based binder in a cylindrical glass shell. The PTFE membrane was selected because it has the highest hydrophobicity among commercial membranes such as polypropylene (PP) and polyvinylidene difluoride (PVDF). It can prevent partial membrane wetting, a phenomenon in which water penetrates the membrane pores and reduces the membrane mass transfer performance [26]. The specifications of the membrane and module used are listed in Table 3.

2-2. The Ammonia Recovery Experiments

Fig. 2 shows a schematic of the membrane contactor setup. Two membrane modules, connected in series, were used for the experiments. The NRP wastewater volumes were 1 L and 0.5 L in the short- and long-term experiments, respectively. The wastewater pH was adjusted to the desired value by using sodium hydroxide (NaOH, KemAus, >97.0%) solution and monitored using a pH meter (Mettler Toledo, Five Easy Plus). After the pH stabilized, the membrane contactor was operated in a circulation configuration in which the wastewater was fed by a peristaltic pump to the membrane module on the shell side and recycled back to the wastewater tank after leaving the second membrane module. The experimental time was recorded after the 0.3 mol/L H_2SO_4 (Ajax Finechem, 98.0% w/w) solution entered the membrane module's tube side. In the long-term operation, the initial TAN concentration of the NRP wastewater was adjusted at the beginning of the experiment using a small amount of solid ammonium chloride (NH_4Cl, KemAus, >99.5%) for the consistency of the mass transfer driving force.

TAN is present in the NRP wastewater in two forms, NH_4^+ and NH_3, according to Eq. (1). The acid dissociation constant (K_a) [27] for the conversion of NH_4^+ to NH_3 can be written as:

$$K_a = \frac{\delta_{NH_3} c_{NH_3} \delta_{H^+} c_{H^+}}{\delta_{NH_4^+} c_{NH_4^+}} = 10^{-\left(0.09+\frac{2,729.92}{T_w}\right)} \quad (2)$$

where δ_i and c_i are the activity coefficients and concentrations of each species, respectively, and T_W is the wastewater temperature.

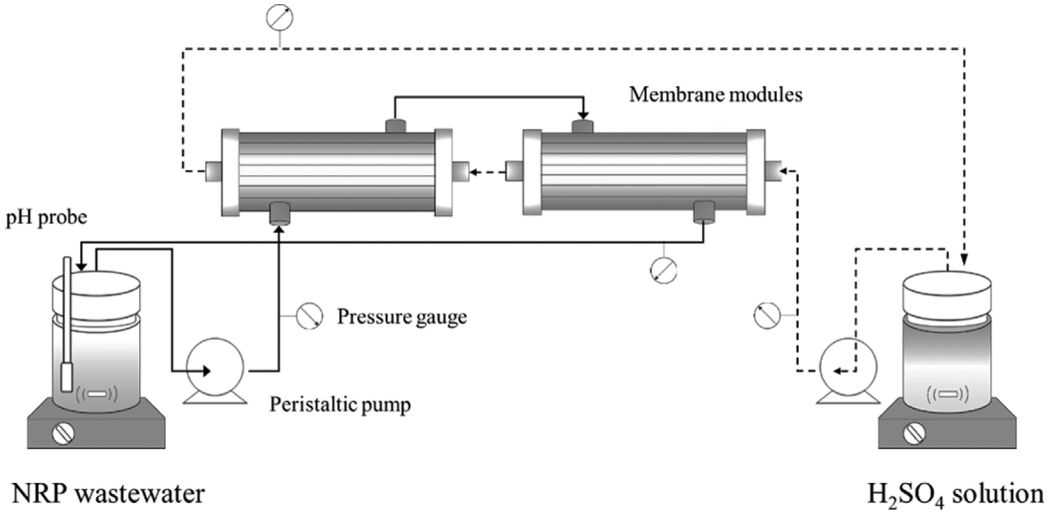

Fig. 2. The hollow fiber membrane contactors' setup for the ammonia recovery from the NRP wastewater.

An equilibrium calculation to determine the fraction of NH_3 to TAN concentration as a function of wastewater pH (derived from Eq. (2)), which was validated by Hafner and Bisogni [28], is presented by the following equation:

$$f_{NH_3} = \frac{c_{NH_3}}{c_{NH_3} + c_{NH_4^+}} = \frac{K_a \delta_{NH_4^+}}{10^{-pH} + \delta_{NH_4^+} K_a} \quad (4)$$

The calculation of $\delta_{NH_4^+}$ in the NRP wastewater is presented in Appendix A, and a value of 0.808 was used in all the calculations.

The NH_3 concentration can be computed from the TAN concentrations, and the mass transfer coefficient of the NH_3 desorption in the circular configuration was calculated based on the reduction of NH_3 concentration with the experimental time using the following equations [29]:

$$c_{NH_3} = f_{NH_3} \cdot c_{TAN} \quad (5)$$

$$K_{OV} = \frac{V}{A \cdot t} \ln \frac{c_{NH_3,0}}{c_{NH_3,t}} \quad (6)$$

where V, A, and t are the wastewater volume (m^3), membrane area (m^2), and operating time (s), respectively. $c_{NH_3,t}$, $c_{NH_3,0}$ and c_{TAN} are the NH_3 at operation time t and its initial value at the start of the experiment and the total NH_3 nitrogen concentration (kmol/m^3), respectively. The c_{TAN} was measured based on the Nessler method using a photometer (HANNA, model HI96733) equipped with a standard solution, and calibration was performed weekly. The data were recorded periodically at 0, 15, 30, and 60 min after the start of the experiments to calculate the K_{OV}. It has been reported that the mass transfer of NH_3 desorption in the wastewater phase is the controlling step in the HMC's system compared with the mass transfer in the membrane and stripping phases [30,31]. Therefore, we focused on investigating the effects of wastewater parameters, including velocity, pH, and TS, on the mass transfer in terms of K_{OV}. The reported K_{OV} is the average value from two replicate experiments and at least three levels of each parameter were studied to assess their effects on the K_{OV}.

3. Foulant Characteristics and Membrane Cleaning Experiment

Several mini-membrane modules consisting of only one hollow fiber with an effective length of 15 cm were continuously fed with NRP wastewater for over 20 days. Only one membrane fiber was used to ensure that the membrane was in full contact with the wastewater. Subsequently, the fouled membrane was removed from the membrane module and cut into small pieces. The foulants on the membrane were observed and characterized by scanning electron microscopy (SEM, Zeiss, Merlin compact), energy dispersive X-ray detection (EDS, Oxford, Aztec), and Fourier-transform infrared spectroscopy (FTIR, Bruker, Tensor27).

To estimate the amount of foulants extracted by the cleaning solutions, the fouled membranes were immersed in the cleaning solution in conical tubes. The tubes were then shaken at 50 rpm in a shaking incubator (Seculite, KS L 2002) for 15 min at 30 °C. The solution was then removed to determine the foulants removed in terms of TS. The remaining foulants were later extracted from the membrane by shaking the tube filled with water at 200 rpm and 30 °C for one hour, followed by handshaking to ensure the complete removal of foulants. The efficiency of the cleaning solution for foulant removal was estimated as the percentage of foulant extracted by the cleaning solution to the total amount of foulant.

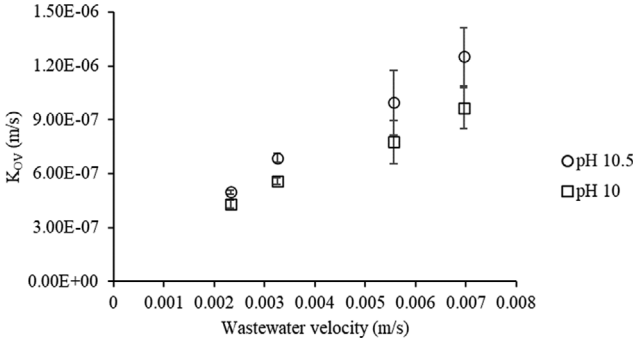

Fig. 3. Effects of wastewater velocity on the K_{OV} of NH_3 desorption from the NRP wastewater at pH 10 and 10.5. The error bars indicate the standard deviation of two replicate experiments.

RESULTS AND DISCUSSION

1. The Performance of the HMC in Short-term Operation

1-1. Effects of Operating Conditions on the K_{OV} of NH_3 Desorption

Actual NRP wastewater with the characteristics shown in Table 2 was used in the experiments, unless otherwise stated. The wastewater was fed into the membrane's shell side, and 0.3 mol/L H_2SO_4 solution at a liquid velocity of 6.5×10^{-3} m/s was flown countercurrently on the tube side of the membrane. Experiments were performed at room temperature (300 K).

The effect of wastewater flow rate on the K_{OV} is shown in Fig. 3. The K_{OV} substantially increased with the wastewater velocity. The mass transfer improved owing to the reduction in the mass transfer resistance of the wastewater phase with an increase in the Reynolds number. In most cases of resource recovery by HMC, wastewater is the dominant mass transfer resistance phase compared to the membrane and stripping solution phases [9]. NH_3 removal by employing the Taguchi approach, Ashrafizadeh and Khorasani [30], reported that the wastewater velocity had a much more significant impact on the K_{OV} than the stripping solution. In this study, the Wilson plot method was employed to confirm the importance of the wastewater phase to overall mass transfer.

The Wilson plot method is based on the mass transfer resistance-in-series for NH_3 desorption and the outer surface of the membrane, as shown in the following equation [32]:

$$\frac{1}{K_{OV}} = \frac{1}{k_w} + \frac{H^*_{NH_3} d_o}{k_m d_{ln}} + \frac{H^*_{NH_3} d_o}{k_s d_i} \quad (7)$$

where k_w, k_m, and k_s are the mass transfer coefficients of the wastewater, membrane, and stripping solution, respectively. Here, d_o, d_{ln}, and d_i are the outside, log mean, and inner diameters of the membrane, respectively. $H^*_{NH_3}$ is the modified Henry's constant considering the dissociation reaction [33].

Yang and Cussler [34] suggested that k_w is a function of $Re^{0.93}$ to obtain a linear relationship between k_W and Re. Therefore, using the straight-line equation (y=mx+c), the intercept of the y-axis (c) from

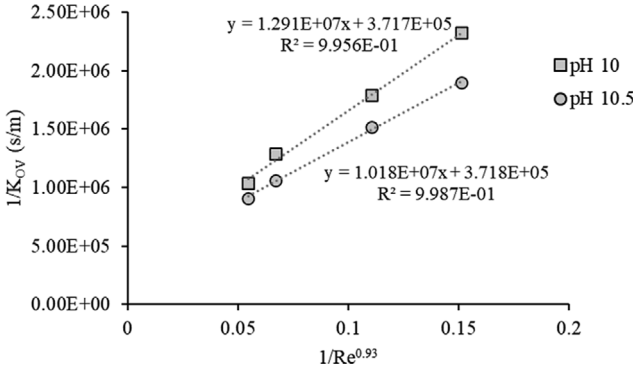

Fig. 4. Wilson plot of NH_3 desorption in the HMC. The intercepts of the y-axis indicate the combined mass transfer resistance of the stripping fluid and membrane phases.

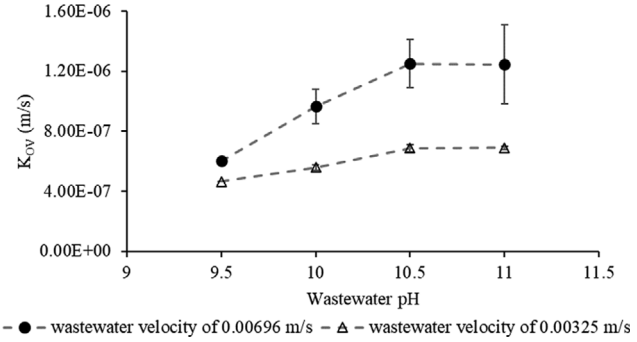

Fig. 5. Effect of wastewater pH on the K_{OV} of NH_3 desorption from the NRP wastewater. The error bars indicate the standard deviation of two replicate experiments.

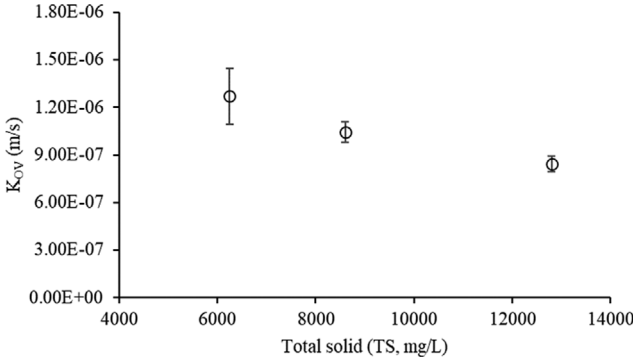

Fig. 6. Effect of wastewater's total solid on the K_{OV} of NH_3 desorption from the NRP wastewater. The wastewater and pH are 6.96×10^{-3} m/s and 10.5, respectively. The error bars indicate the standard deviation of two replicate experiments.

the plot between $1/K_{OV}$ (y) and $1/Re^{0.93}$ (x) represents the combined mass transfer resistance of the membrane and stripping solution phases ($\frac{H^*_{NH_3}d_o}{k_m d_{ln}} + \frac{H^*_{NH_3}d_o}{k_s d_i}$). Substitution of the intercept value into Eq. (6) also provides the mass transfer resistance of the wastewater phase ($1/k_W$). Wilson's plot in Fig. 4 shows that the combined mass transfer resistances of the membrane and stripping solution phases of the wastewater at pH 10.5 and 10 were 4.37×10^5 and 4.54×10^5 s/m, respectively. Under these conditions, the mass transfer resistance of the wastewater phase ($1/k_W$) was higher at 5.54×10^5 s/m and 5.81×10^5 s/m for wastewater pH of 10.5 and 10, respectively. These results verified that the resistance of the wastewater phase controlled NH_3 desorption from NRP wastewater. The significance of the mass transfer resistances of the combined membrane and stripping solution increased with the wastewater pH. This was due to the increase in gaseous NH_3 concentration at the interface between the wastewater and membrane phases, improving the mass transfer in the membrane phase and reducing the significance of the wastewater phase.

The NRP wastewater was initially in an acidic condition (pH ~2.5) owing to the addition of acid (H_2SO_4 or formic acid) to the natural latex as a coagulant for the aggregation of rubber. The reaction of acids and NH_3 was also the reason for the substantial amount of dissolved NH_3 in NRP wastewater. Under these conditions, the dissolved NH_3 was in the form of NH_4^+, which the HMC process removed poorly. Thus, the NRP wastewater required pH adjustment, and NaOH solution was employed in this study. The effects of the pH of the NRP wastewater on K_{OV} are shown in Fig. 5. The K_{OV} of both wastewater velocities improved substantially with wastewater pH from 9.5 to 10.5. The increase in pH enhanced the conversion of NH_4^+ to NH_3 according to Eq. (1), improving the mass transfer driving force and, consequently, the mass transfer coefficients. The increase in wastewater pH from 10.5 to 11 slightly affected the K_{OV}s as most of the NH_4^+ had already been converted to NH_3 at pH 10.5. Thus, there was no significant change in the mass transfer driving force between pH 10.5 and 11. The range of the K_{OV} obtained was also compared with those of other studies to confirm the reliability of the data, as shown in Table 4. The K_{OV} of our study was in the same range as some studies and slightly below others, which was possibly due to the lower wastewater velocity used in our experiments.

Table 4. Comparison of the overall mass transfer coefficients (K_{OV}) of the ammonia desorption in the HMC's system reported in the literature

Works	Membrane	pH range	Liquid velocity	K_{OV} (m/s)
Ashrafizadeh and Khorasani [30]	PP	8-11	0.053 m/s	$1.206\text{-}11.79\times10^{-6}$
Baumann and Fuchs [20]	PP	8-10	-	$0.75\text{-}5.08\times10^{-6}$
Lui and Wang [35]	PVDF	11.5	0.0048-0.248 m/s	$5.5\text{-}8.9\times10^{-6}$
Ahn et al. [36]	PTFE	11	10-20 ml/min	$1.5\text{-}3.06\times10^{-6}$
Present study	PTFE	9-11	0.0067 m/s (75 ml/min)	$0.61\text{-}1.25\times10^{-6}$

- not reported

The effect of TS in the wastewater phase on the mass transfer coefficient of NH_3 desorption is shown in Fig. 6. The wastewater velocity and pH were 6.96×10^{-3} m/s and 10.5, respectively. Wastewater TS increased by mixing the wastewater with sediments from a similar type of wastewater. The results show that the increase in the TS reduced the K_{OV}. This was due to a portion of the dissolved NH_4^+ and NH_3 being bonded and attached to the solid particles suspended in the wastewater phase, reducing NH_3 volatilization [37]. Thus, the NH_3 desorption coefficient decreased with the TS. The same phenomenon was observed by Vaddella et al. [38], who investigated the mass transfer coefficient of NH_3 from dairy manure using an air stripping method. Vaddella et al. [38] also presented an empirical correlation of the acid dissociation constant (K_a) as a function of the total solid concentration as $K_a=10^{-(2.0153+1.208\times TS)\left(1.8944+\frac{819.8}{T_W}\right)}$ (where TS is the total solids in units of (%w/w)/100). Using this correlation, the K_a values of the wastewater containing TS of 6,250 mg/L and 12,800 mg/L were 5.41×10^{-3} and 4.81×10^{-3}, respectively. The decrease of K_a means the decrease in NH_3 volatilization in accordance with Eq. (2). The same parameter was used to describe the difference in NH_3 volatilization between swine anaerobic lagoon liquid and deionized water by Arogo et al. [39].

1-2. Recovery Efficiency

The HMC's ability to remove 90% of TAN from the NRP wastewater was tested, and the results are shown in Fig. 7. The experiments were operated in a circulation configuration with a wastewater volume of 0.5 liters to shorten the experiments' time. The volume of the acid solution was one liter to ensure the lowest NH_3 concentration on the stripping side. The wastewater pH was periodically adjusted to be maintained at 10.5. The y-axis denotes the ratio of the total NH_3 concentration at the recorded experimental time to its initial value at time 0 ($c_{TAN,t}/c_{TAN,0}$). A 90% removal of TAN could be achieved at all the wastewater flow rates. The required time was quite long because of the small membrane area used in the experiments. However, they decreased as the wastewater velocity increased. It was also noticed that the TAN concentration decreased relatively slowly after the 80% removal. This was due to the low mass transfer driving force, as the remaining NH_3 concentration was minimal. It should also be noted that the experimental time could be further reduced by increasing the membrane area after adding more fibers or expanding the membrane length. The increase in the interfacial area between the wastewater and stripping solution enhanced the contact time between the two phases and improved the amount of dissolved NH_3 removed from the wastewater phase.

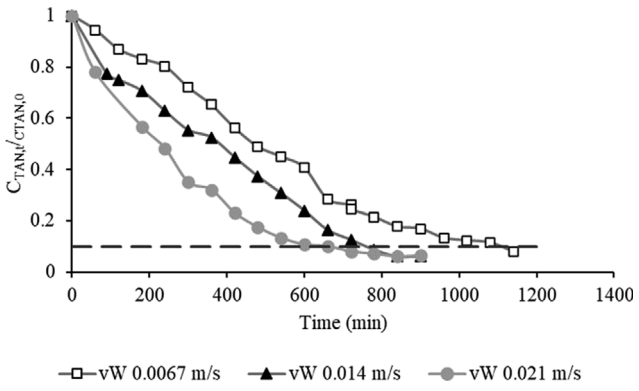

Fig. 7. The ratio of total ammonia concentration at recorded experimental time and its initial value at the start of experiments of different wastewater velocities (v_W).

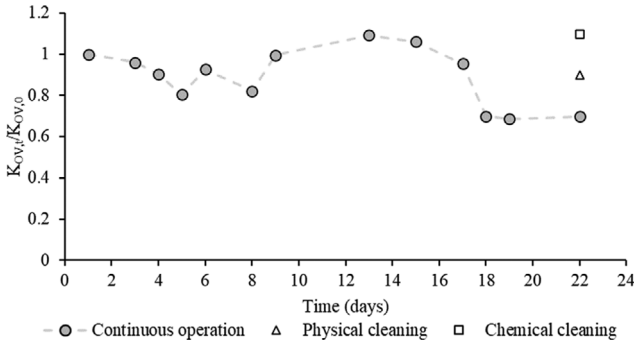

Fig. 8. The mass transfer coefficient of NH_3 desorption at the experimental time ($K_{OV,t}$) compared with the initial value at the start of the experiment ($K_{OV,0}$) in the long-term operation with NRP wastewater. The physical and chemical membrane cleanings were conducted by flushing with water and with a series of 0.1 mol/L NaOH and 0.1 HCl solutions, respectively.

2. The Performance of the HMC in Long-term Operations

2-1. The Observed Mass Transfer Coefficients in Long-term Operation

The long-term performance over 20 days of the HMC in terms of K_{OV} for the recovery of NH_3 from NRP wastewater is shown in Fig. 8. The NRP wastewater was continuously fed to the membrane modules for the entire operation at velocity of 6.96×10^{-3} m/s. In contrast, the acid solution was fed at 6.5×10^{-3} m/s to the lumen side only when conducting measurements of K_{OV} (besides that, the distilled water at the same velocity was fed). The wastewater was replaced every two days, and a fresh acid solution was used in every experiment. At the beginning of the experiment, the initial TAN concentrations were adjusted to approximately 650 mg/L to ensure the consistency of the initial mass transfer driving force in every experiment. The y-axis is the ratio between the measured K_{OV} at a certain time t and its initial values at the start of the experiment ($K_{OV,t}/K_{OV,0}$).

It can be observed from Fig. 8 that the K_{OV} did not have a noticeable change during the first 15 days, and after which it continuously declined until it was roughly 70% of its initial value after 22 days. The results show that HMC has a low membrane fouling tendency compared to pressurized filtration membrane processes, in which the flux decline can be observed in the duration of hours [40]. The K_{OV} decline in the HMC was due to the deposition of the fouling layer on the membrane surface, which introduced extra mass transfer resistance to NH_3 desorption. The foulant gradually accumulated on the membrane surface over time, resulting in a continuous reduction in the K_{OV}.

Membrane cleaning was performed after 22 days of continuous operation. First, physical membrane cleaning with deionized water was tested by feeding it in the opposite direction to the waste-

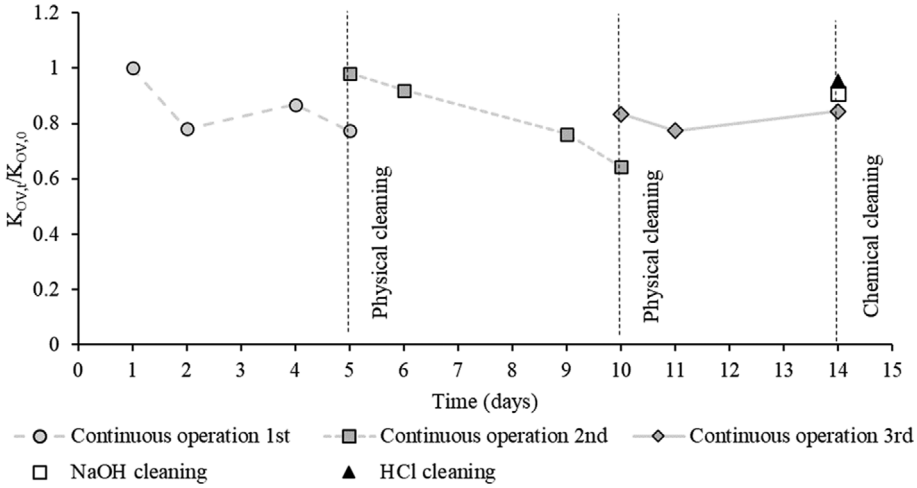

Fig. 9. The mass transfer coefficient of NH_3 desorption at the experimental time ($K_{OV,t}$) compared with the initial value at the start of the experiment ($K_{OV,0}$) in the second long-term operation with NRP wastewater.

water at a liquid velocity of 6.96×10^{-2} m/s for one hour. The membrane was then dried using an air pump prior to the NH_3 desorption experiments. The physical cleaning could only restore the mass transfer coefficient to 90.02% of its initial value. Because the performance of the HMC could not be fully restored, the membrane underwent a series of chemical membrane cleaning procedures. It was first washed with water at a velocity of 6.96×10^{-2} m/s for 30 min, followed by 0.1 mol/L NaOH and 0.1 HCl solution, respectively, at the same flow rate for one hour each. This series of membrane cleaning was designed based on the suggestion of Veerasamy and Ismail [41], who studied the membrane cleaning of an ultrafiltration process for natural latex concentration. After chemical cleaning, the K_{OV} returned close to its initial value. The differences in physical and chemical cleaning performance suggested that the foulants could be strongly bonded on the membrane surface owing to long-term operation.

The second long-term operation of the HMC for the recovery of NH_3 was performed to evaluate the cleaning solution type, and the results are shown in Fig. 9. The inlet TAN concentration, wastewater, and acid solution flow rates were the same as those used in a previous experiment. It was observed that the K_{OV} decreased about 25% after five days of operation. The K_{OV} was restored after physical cleaning using water at a liquid velocity of 6.96×10^{-2} m/s for 1 h. The decline of the K_{OV} in the first five days was also observed in the first long-term operation, as shown in Fig. 8. Nevertheless, it also improved after the experiment was continued. It is possible that the fouling that occurred during the first five days of the experiments was caused by small foulant particles with weak adhesion forces toward the hydrophobic membrane surface. These tiny particles, which were aggregated on the membrane surface, later became larger and easier to wash off from the membrane surface by the physical forces from the water cleaning or the wastewater flowing, resulting in the recovery of the K_{OV}.

However, cleaning by physical forces cannot remove all the foulants attached. The K_{OV} decline between the sixth and tenth days of the operation after the first physical cleaning was more severe than that of the first five days. The K_{OV} was only 64.2% of its initial value after the ten days of operation. The remaining foulant contributed to additional mass transfer resistance and decreased the contact angle of the membrane surface, inducing the wetting phenomenon [42], which further deteriorated the K_{OV} even further. In addition, the interactions between the remaining foulants on the membrane surface and foulants in the liquid bulk are greater than those between the foulants in the liquid bulk and the membrane material [43]. Therefore, if physical cleaning fails to remove all the membrane foulants, membrane fouling occurs faster. The second physical cleaning, which was applied after ten days of operation, failed to return the K_{OV} to its initial value, with K_{OV} merely at 83.3%. Abdel-Karim et al. [44] reported that repeated physical membrane cleaning could lead to more severe membrane fouling, as evidenced by the poor recovery of the contact angle of the membrane surface. The effectiveness of 0.1 M NaOH solution as the cleaning agent was tested after the experiment was conducted for 14 days, and the K_{OV} was at 84.5% of the initial value. The NaOH solution was fed at a liquid velocity of 6.96×10^{-2} m/s for 1 h. After the cleaning, the K_{OV} recovered back to 91% of its initial value. This suggests that the foulants comprised organic compounds that could be dissolved in the alkali solution. After NaOH washing, acid cleaning with 0.1 M HCl was performed using the same flow rate and duration. The acid cleaning further increased the K_{OV} to almost its initial value (95.1%). Because acid solutions are known to be effective in inorganic foulant cleaning, the foulants in this work might also contain some inorganic salts. The acid can dissolve and loosen the precipitates from the inorganic foulant, making it easier to remove the foulant from the membrane substrate.

2-2. Efficiency of Membrane Cleaning Solutions

Mini-membrane modules with an effective length of 15 cm were fed continuously by NRP wastewater at 6.96×10^{-3} m/s for 20 days. The fouled membranes were removed from the module and immersed in the cleaning solution (deionized water, 0.1 mol/L HCl, and 0.1 mol/L NaOH). The membrane and cleaning solution were shaken at 50 rpm for 15 min, and then TS measurements on the cleaning solution were performed. The total TS content of the foulant was estimated after the remaining foulant was extracted. Fig.

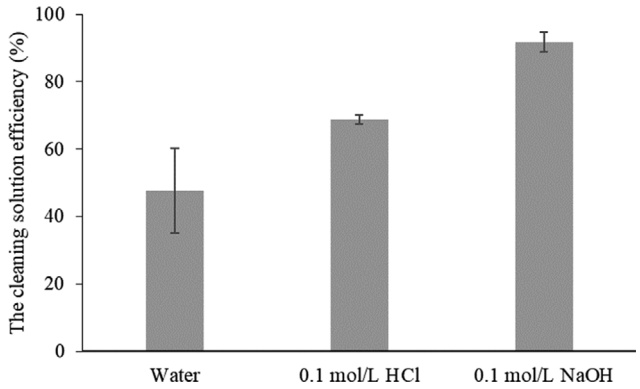

Fig. 10. The efficiency of membrane cleaning solutions in extracting the foulants.

10 shows the efficiency of the cleaning solution in terms of the ratio between the TS of foulants extracted by a cleaning solution and the TS of the foulants on the membrane surface.

It can be seen that the NaOH solution was the most effective cleaning solution, and it could remove almost 92% of the foulants in terms of TS. Although the efficiency of the HCl solution was lower than that of the NaOH solution, it was higher than that of the deionized water. The higher efficiency of the NaOH solution suggests that the majority of foulants were organic compounds. The chemical bonds of the organic foulants can be broken down in a high-pH solution. The organic particles decomposed into smaller particles, making it easier to remove the foulant [45]. The findings in our study agree with the results of Veerasamy and Ismail using a PVDF ultrafiltration membrane with NRP wastewater [41], where the alkali solution was found to be the most efficient cleaning solution compared to an acid solution and water.

3. Fouling Investigation

3-1. Membrane Autopsy and Foulant Characterization

In a separate experiment, two mini membrane modules consisting of only one hollow fiber with an effective length of 15 cm were constructed and fed with NRP wastewater at a liquid velocity of 6.96×10^{-3} m/s for 22 days. The fouled membranes were then carefully removed from the membrane module for characterization.

The scanning electron microscope (SEM) images of the outer surfaces of the fouled and new membranes are compared in Fig. 11(a) and (b). The figures show the changes in the membrane surface morphology between the fouled and new membranes. The fouled membrane is covered with an amorphous and uneven layer of foulants. It can also be noticed that there are two types of fouled surfaces: the smooth part (the middle of Fig. 11(b)) and the rough area made of conglomerate particles (the upper right and bottom center of Fig. 11(b)). Cross-sectional images of the fouled mem-

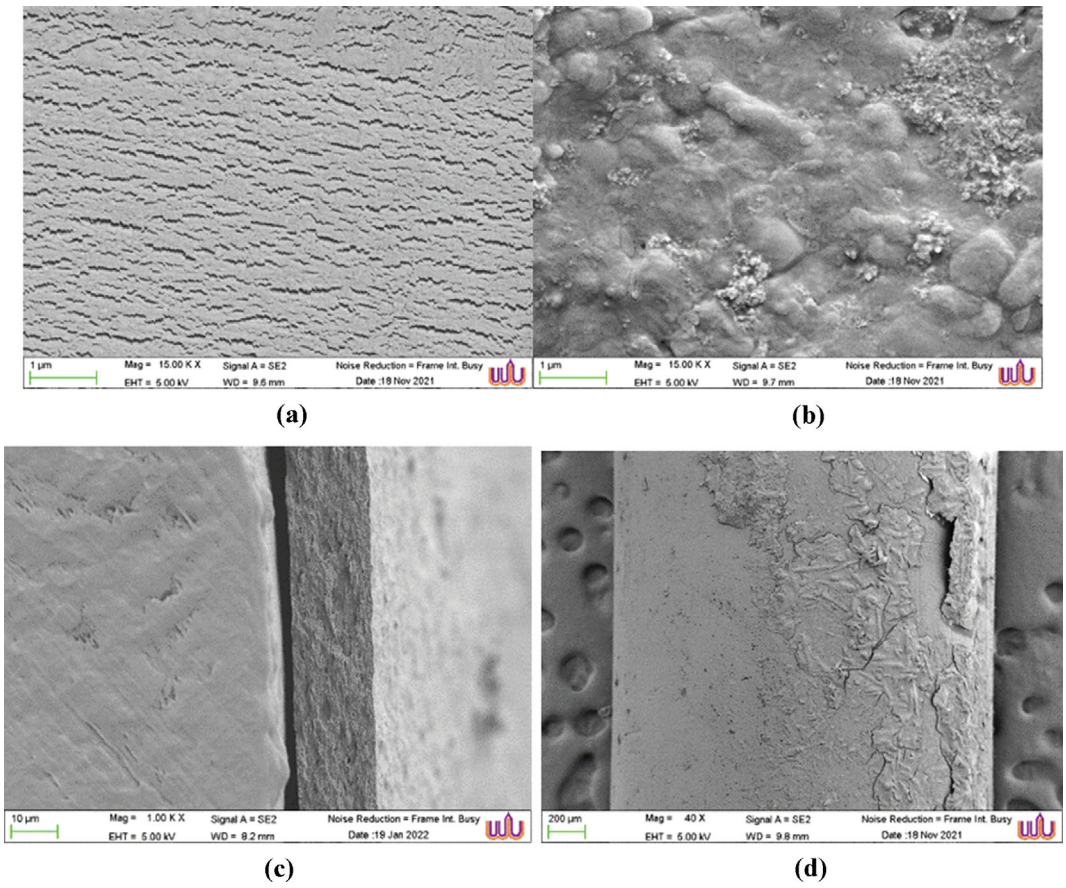

Fig. 11. SEM images of (a) outer surface of the new PTFE membrane, (b) outer surface of the fouled membrane, (c) cross-section of the fouling layer and membrane substrate, (d) outer surface of a fouled membrane.

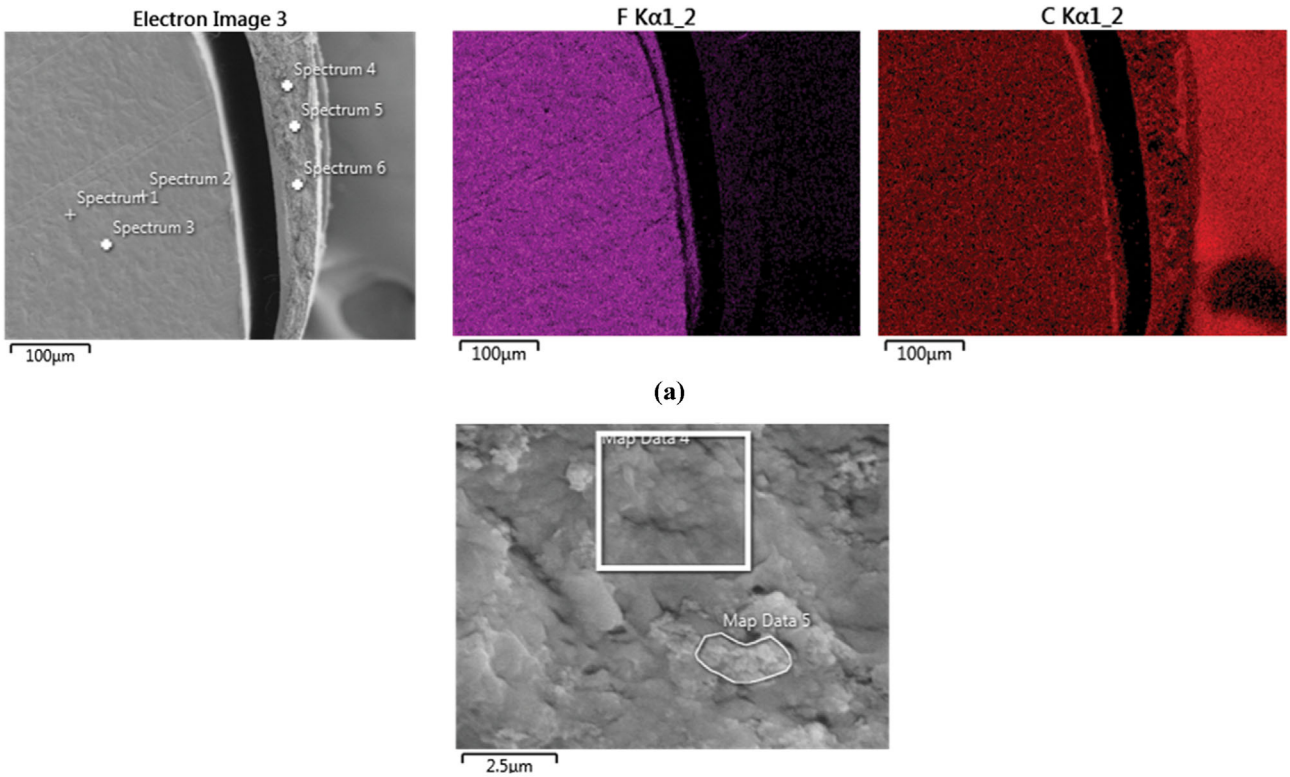

Fig. 12. SEM/EDS images of (a) cross-section of the fouled membrane with F and C elemental mapping, (b) outer surface of the fouled membrane, indicating the mapping area of the smooth area (rectangular) and conglomerate area (irregular octagon).

Table 5. Elemental composition of foulants measured by EDS

Elements	C	F	O	N	Na	S	Cl	P	Zn	Ca	Fe	K	Cu	Al	Mg
Cross section (%)	54.78	2.62	17.94	4.23	4.36	3.83	2.80	1.64	2.80	1.84	0.99	0.92	0.72	0.67	0.19
Outer surface															
Smooth area (%)	39.03	0.02	22.43	3.83	4.75	3.44	2.37	4.06	9.81	1.79	2.06	1.42	0.86	1.07	0.50
Conglomerate area (%)	24.76	0.00	30.57	0.00	6.36	3.00	2.88	5.50	13.83	2.08	1.97	1.70	0.87	1.97	0.76
PTFE (%)	38.26	61.74	-	-	-	-	-	-	-	-	-	-	-	-	-

Data reported were averaged of at least six points

branes are shown in Fig. 11(c) at 1,000x magnifications. It is apparent that a dense and uniform cake layer developed on the membrane surface, and there was no evidence of foulants penetrating the membrane substrate. The zoomed-out image of the outer membrane surface (Fig. 11(d)) shows that the fouled layer covers only a part of the membrane surface. The incomplete cover of the foulants on the membrane surface suggests that the membrane may be initially fouled by the intermediate pore-blocking mechanism, followed by cake formation over the blocked regions, which is also evident from the uneven foulant surface shown in Fig. 11(b). Ramezanianpour and Sivakumar [46] also proposed that fouling in the membrane distillation process (an HMC in which water is the target transferring species) occurs from more than one type of fouling mechanism and is also from intermediate pore blocking followed by cake formation.

SEM/EDS images of the fouled membranes are shown in Fig. 12. The SEM/EDS images confirm the forming of the cake layer on the membrane surface as the elemental signal of fluorine (F) of the PTFE membrane was in a clear difference in the density compared to that of the cake foulant layer in Fig. 12(a). The images also indicate that the cake layer consisted of carbon (C), implying that the foulant layer consisted of organic compounds.

The elemental composition analysis by SEM/EDS of the foulant layer and membrane substrate in the cross-sectional image (Fig. 12(a)) and outer surface (Fig. 12(b)) are summarized in Table 5. The elemental compositions show that the distinctive difference between the PTFE membrane substrate and foulants was the presence of metal ions. These metal ions are natural latex components [47] and chemicals added to natural rubber production. The metal ions not being detected in the membrane substrate suggest that there was no foulant penetration into the membrane pores, and that the foulant was formed only as a cake layer, as shown in Fig.

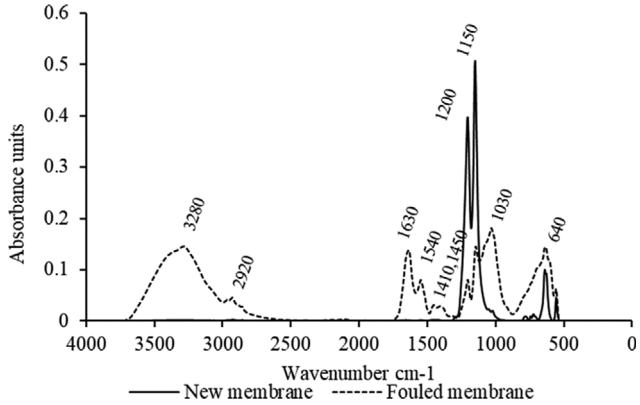

Fig. 13. FTIR spectra of a new and fouled PTFE membrane.

11(c). Elemental analysis of the foulant in the cross-section and outer surface showed high Zn^{2+} content from zine oxide, an anti-coagulant, and preservative of the natural latex. There were also significant portions of negative discharge S^{2-} and Cl^{-} from sulfuric acid (a coagulant agent) and chlorine (a chemical additive and disinfectant agent). These elements (Zn^{2+}, S^{2-}, and Cl^{-}) developed inorganic salts (sulfate and chloride salts) on the membrane surface, which is why the acid solution was quite effective in membrane cleaning.

Elemental analysis of the foulant cross-section revealed a significantly higher O content than that of the PTFE membrane substrate. This implies that proteins that are non-rubber components in natural latex [48] could be a constituent of the cake fouling layer. Proteins have a strong affinity for hydrophobic membrane [49]. Therefore, they can be deposited and attached to the membrane surfaces. This result revealed that some of the foulant was from the uncoagulated latex in the wastewater. Two types of fouled surfaces, the smooth and conglomerate areas observed in the SEM images, were separately analyzed and compared. Interestingly, N atoms were absent in the conglomerate area. The conglomerate particles on the membrane surface may also be caused by the deposition of uncoagulated natural latex. However, the latex proteins could be degraded and washed away because of the alkali conditions [50] induced by NH_3 desorption.

The FTIR spectra of the new and fouled membranes are shown and compared in Fig. 13. The spectra of the fresh PTFE membrane show absorption bands at wavenumbers of 640 cm^{-1}, 1,150 cm^{-1} and 1,200 cm^{-1}, which belong to the CF_2 groups of PTFE [51]. The fouled PTFE membrane exhibits several additional bands compared to those of the fresh membrane. The broad band at 3,200 cm^{-1} corresponding to the O-H group indicates the presence of organic compounds. The bands at 1,630 and 1,540 cm^{-1} correspond to amide bonds in NR proteins [52]. These results confirm the finding from the SEM/EDS, which showed foulants on the membrane surface are organic compounds composed of proteins that belong to the uncoagulated NR. In addition, the absorption band at 1,030 cm^{-1} is attributed to the sulfonyl group (S=O), implying the decomposition of inorganic sulfate compounds on the membrane surface [53]. The FTIR spectra of the other major non-rubber compounds, including lipids and carbohydrates, were not observed because there were no peaks at 1,748-1,738 cm^{-1} and 1,711 cm^{-1} associated with the ester and carboxyl groups of the lipid and carbohydrate molecules [52].

3-2. Proposed Fouling Mechanism

This section proposes a fouling mechanism that possibly results in cake layer formation during NH_3 desorption in the HMC, as illustrated in Fig. 14. The proteins, organic compounds, and traces of metal ions observed in Section 3.3.1 suggest that the primary foulant was from the uncoagulated NR particles, the main contaminant of the NRP wastewater.

NR particles with negative charges on the outside are covered by a matrix layer of proteins and phospholipids [54]. The covered proteins have a strong adhesion force toward the hydrophobic surfaces [55]; therefore, the natural rubber particles could be deposited on the PTFE membrane surface even though there was no pressure difference between the wastewater and stripping solution applied in the HMC process. The proteins could also act as a supporting framework for accumulating rubber particles [56], which later grew into a cake fouling layer. At the same time, the negative surface charge of NR particles was able to cross-link with other rub-

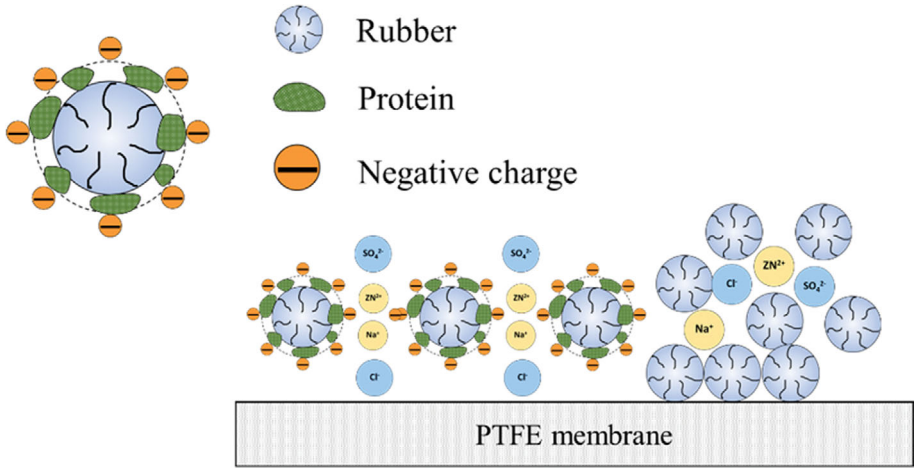

Fig. 14. Proposed fouling mechanism in the HMC during the NH_3 desorption.

ber particles by ionic bonding via positive ions such as Zn^{2+} and Na^{+}, forming larger rubber particles [57] and allowing inorganic salts to be embedded in-between. The accumulation of the NR particles via this mechanism could result in a fouling layer comprising all the proteins and organic and inorganic compounds detected in the SEM/EDS and FTIR analyses.

Interestingly, the fouling layer also contained conglomerate areas, where the evident N atoms from the protein substance were absent. The area could also be developed from uncoagulated NR particles. However, the proteins were degraded owing to the alkali conditions induced by the presence of NH_3 [50] during desorption. As the covered proteins were washed away, the fouling layer became a conglomerate of rubber and inorganic salts, as evidenced by SEM/EDS.

CONCLUSION

The mass transfer of NH_3 desorption from NRP wastewater by HMC was investigated in this study. The main findings of our study are as follows:

In the short-term experiments

- The NH_3 desorption mass transfer coefficient increased with wastewater velocity and pH, but decreased when the amount of TS in NRP wastewater increased.
- Wilson's plot method confirmed that the wastewater phase plays the most dominant role in the mass transfer of NH_3 desorption.
- HMC could remove 90% of the total ammonia concentration from the NRP wastewater.

In the long-term experiments

- The HMC could be operated for at least 15 days without a permanent decline in the mass transfer coefficient owing to membrane fouling.
- Chemical cleaning using deionized water, NaOH (0.1 M), and HCl (0.1 M HCl, consecutively, could recover the mass transfer coefficient, but physical cleaning (flushing) using only a high flow rate of water failed to do so.
- Fouling characterization revealed that the uncoagulated NR particles created a cake layer and allowed the inorganic salts to be embedded during NH_3 desorption.

ACKNOWLEDGEMENTS

This work was financially supported by Office of the Permanent Secretary, Ministry of Higher Education, Science, Research, and Innovation (Thailand) through grant RGNS 63-214 and the new strategic research project (P2P) fiscal year 2022, Walailak University, Thailand.

CONFLICT OF INTEREST

The authors declare no conflict of interest.

REFERENCES

1. FAOSTAT, Countries by commodity (Rubber, natural), https://www.fao.org/faostat/en/#rankings/countries_by_commodity, Access date January 2021.
2. W. Jawjit, C. Kroeze and S. Rattanapan, *J. Clean. Prod.*, **18**, 403 (2010).
3. P. Tekasakul and S. Tekasakul, *J. Aerosol Sci.*, **21**, 122 (2006).
4. G. Zhu, Y. Peng, B. Li, J. Guo, Q. Yang and S. Wang, *Rev. Environ. Contam. Toxicol.*, **192**, 159 (2008).
5. H. J. Al-Jaaf, N. S. Ali, S. M. Alardhi and T. M. Albayati, *Desalin. Water Treat.*, **245**, 226 (2022).
6. S. T. Kadhum, G. Y. Alkindi and T. M. Albayati, *Desalin. Water Treat.*, **231**, 44 (2021).
7. W. Jawjit, P. Pavasant and C. Kroeze, *J. Clean. Prod.*, **98**, 84 (2015).
8. D. Tanikawa, T. Kataoka, Y. Hirakata, M. Hatamoto and T. Yamaguchi, *Process Saf. Environ. Protect.*, **138**, 256 (2020).
9. W. Rongwong and K. Goh, *J. Environ. Chem. Eng.*, **8** 104242 (2020).
10. A. Gabelman and S. T. Hwang, *J. Membr. Sci.*, **159**, 61 (1999).
11. Y. Xu, K. Goh, R. Wang and T. H. Bae, *Sep. Purif. Technol.*, **229** 115791 (2019).
12. D. Tanikawa, T. Kataoka, Y. Hirakata, M. Hatamoto and T. Yamaguchi, *Process Saf. Environ. Protect.*, **138**, 256 (2020).
13. M. Mohammadi, H. C. Man, M. A. Hassan, P. L. Yee, *Afr. J. Biotechnol.*, **9**, 6233 (2010).
14. N. Nasir, Z. Daud, A. A. Kadir, A. A. A. Latiff, B. Ahmad, N. Suhani, H. Awang, A. A. Oyekanmi and A. A. Halim, *Malaysian J. Fundam. Appl. Sci.*, **15**, 862 (2019).
15. A. Masoud Samani Majd and S. Mukhtar, *Trans. ASABE*, **56**, 1951 (2013).
16. M. C. Garcia-González and M. B. Vanotti, *Waste Manag.*, **38**, 455 (2015).
17. M. Fillingham, A. VanderZaag, J. Singh, S. Burtt, A. Crolla, C. Kinsley and J. D. MacDonald, *Membranes*, **7**, 59 (2017).
18. J. Zhang, M. Xie, X. Tong, S. Liu, D. Qu and S. Xiao, *Sep. Purif. Technol.*, **239**, 116579 (2020).
19. M. B. Vanotti, P. J. Dube, A. A. Szogi and M. C. García-González *Water Res.*, **112**, 137 (2017).
20. F. Wäeger-Baumann and W. Fuchs, *Sep. Sci. Technol.*, **47**, 1436 (2012).
21. M. J. Rothrock, A. A. Szögi and M. B. Vanotti, *Waste Manage.*, **33**, 1531 (2013).
22. P. H. Lin, R. Y. Horng, S. F. Hsu, S. S. Chen and C. H. Ho, *Int. J. Environ. Res. Public Health*, **15**, 441 (2018).
23. B. Brennan, J. Lawler and F. Regan, *Environ. Sci. Water Res. Technol.*, **7**, 259 (2021).
24. M. C. S. Amaral, N. C. Magalhães, W. G. Moravia and C. D. Ferreira, *Water Sci. Technol.*, **74**, 2177 (2016).
25. Federation, Water Environmental, and APH Association. APHA: Washington, DC, USA 21 (2005).
26. S. Khaisri, D. deMontigny, P. Tontiwachwuthikul and R. Jiraratananon, *Sep. Sci. Technol.*, **65**, 290 (2009).
27. Florida Department of Environmental Protection, Chemistry Laboratory Methods Manual, Tallahassee, 12 (2001).
28. S. D. Hafner and J. J. Bisogni, *Water Res.*, **43**, 4105 (2009).
29. Z. Zhu, Z. Hao, Z. Shen and J. Chen, *J. Membr. Sci.*, **250**, 269 (2005).
30. S. N. Ashrafizadeh and Z. Khorasani, *Chem. Eng. J.*, **162**, 242 (2010).
31. X. Tan, S. P. Tan, W. K. Teo and K. Li, *J. Membr. Sci.*, **271**, 59 (2006).
32. W. Rongwong and S. Sairiam, *J. Environ. Chem. Eng.*, **8**, 104240 (2020).

33. G. K. Agrahari, S. K. Shukla, N. Verma and P. K. Bhattacharya, *J. Membr. Sci.*, **390-391**, 164 (2012).
34. M. C. Yang and E. L. Cussler, *AIChE J.*, **32**, 1910 (1986).
35. H. Liu and J. Wang, *Prog. Nucl. Energy*, **86**, 97 (2016).
36. Y. T. Ahn, Y. H. Hwang and H. S. Shin, *Water Sci. Technol.*, **63**, 2944 (2011).
37. A. D. Visscher, L. A. Harper, P. W. Westerman, Z. Liang, J. Arogo, R. R. Sharpe and O. V. Cleemput, *J. Appl. Meteorol. Climatol.*, **41**, 426 (2002).
38. V. K. Vaddella, P. M. Ndegwa, J. L. Ullman and A. Jiang, *Atmos. Environ.*, **66**, 107 (2013).
39. J. Arogo, P. W. Westerman and Z. S. Liang, *Trans ASABE*, **46**, 1415 (2003).
40. S. Hube, M. Eskafi, K. F. Hrafnkelsdóttir, B. Bjarnadóttir, M. Á. Bjarnadóttir, S. Axelsdóttir and B. Wu, *Sci. Total Environ.*, **710**, 136375 (2020).
41. D. Veerasamy and A. Ismail, *Desalination*, **286**, 235 (2012).
42. M. M. Damtie, B. Kim, Y. C. Woo and J.-S. Choi, *Chemosphere*, **206**, 793 (2018).
43. J. Teng, M. Zhang, K. T. Leung, J. Chen, H. Hong, H. Lin and B. Q. Liao, *Water Res.*, **149**, 477 (2019).
44. A. Abdel-Karim, S. Leaper, C. Skuse, G. Zaragoza, M. Gryta and P. Gorgojo, *Chem. Eng. J.*, **422**, 129696 (2021).
45. Z. Wang, J. Ma, C. Y. Tang, K. Kimura, Q. Wang and X. Han, *J. Membr. Sci.*, **468**, 276 (2014).
46. M. Ramezanianpour and M. Sivakumar, *Desalination*, **345**, 1 (2014).
47. M. M. Rippel, C. A. Paula Leite and F. Galembeck, *Anal. Chem.*, **74**, 2541 (2002).
48. L. Tarachiwin, J. Sakdapipanich and Y. Tanaka, *Rubber Chem. Technol.*, **76**, 1185 (2003).
49. R. Miao, L. Wang, N. Mi, Z. Gao, T. Liu, Y. Lv, X. Wang, X. Meng and Y. Yang, *Environ. Sci. Technol.*, **49**, 6574 (2015).
50. F. W. Perrella and A. A. Gaspari, *Methods*, **27**, 77 (2002).
51. W. U. Rehman, A. Muhammad, M. Younas, C. Wu, Y. Hu and J. Li, *J. Membr. Sci.*, **584**, 66 (2019).
52. S. Rolere, S. Liengprayoon, L. Vaysse, J. Sainte-Beuve and F. Bonfils, *Polym. Test.*, **43**, 83 (2015).
53. MERCK, IR spectrum table & chart, URL: https://www. sigmaaldrich. com/technical-documents/articles/biology/ir-spectrum-table. html, Access date January 2021 (2020).
54. C. N. Rochette, J. r. m. J. Crassous, M. Drechsler, F. Gaboriaud, M. Eloy, B. de Gaudemaris and J. r. m. F. Duval, *Langmuir*, **29**, 14655 (2013).
55. M. Malmsten, *Colloids Surf. B Biointerfaces*, **3**, 297 (1995).
56. M. Sriring, A. Nimpaiboon, S. Kumarn, K. Higaki, Y. Higaki, K. Kojio, A. Takahara, C. C. Ho and J. Sakdapipanich, *Colloids Surf. A: Physicochem. Eng. Asp.*, **592**, 124571 (2020).
57. K. Berthelot, S. Lecomte, Y. Estevez, V. Zhendre, S. Henry, J. Thévenot, E. J. Dufourc, I. D. Alves and F. Peruch, *Biochim. Biophys. Acta Biomembr.*, **1838**, 287 (2014).

Appendix A Calculation of the Activity Coefficient of NH_4^+

The ionic strength (I) of the ions in the NRP wastewater from the concentration and valence (Z) in the solution were:

$$I=\frac{1}{2}\Sigma_i c_i Z_i^2=\frac{1}{2}(c_{SO_4^{2-}}\cdot -2^2+c_{Zn^{2+}}\cdot 2^2+c_{Ca^{2+}}\cdot 2^2 + c_{Fe^{2+}}\cdot 2^2+c_{Cu^{2+}}\cdot 2^2+c_{K^+}\cdot 1^2)$$

Using the data from Table 2, the ionic strength of NRP wastewater was 0.051 mol/L;

Then, the activity coefficient was calculated with the equation of Güntelberg as follows:

$$\delta=10^{-\frac{0.5\cdot Z^2\sqrt{I}}{1+\sqrt{I}}}$$

The activity coefficient of the ammonium ion ($\delta_{NH_4^+}$) is then:

$$\delta_{NH_4^+}=10^{-\frac{0.5\cdot 1^2\sqrt{0.051}}{1+\sqrt{0.051}}}=0.808$$